技術ノート

前進飛行中のヘリコプタ・ロータおよびロータと胴体の干渉に関する空力シミュレーション

Aerodynamic Simulation of a Helicopter Rotor in Forward Flight and of Rotor / Body Interference

川 田 忠 裕*
Tadahiro KAWADA

In this study, an unsteady panel method code was verified and its applicability to helicopter aerodynamics was studied. The code uses a vortex wake method along with a low order panel method, PMARC. The code has a major advantage in that complex wake shapes are automatically developed so that the prescription of wake shapes as required by other methods is not necessary. The code could predict the unsteady aerodynamic forces for a sudden forward motion and a pitching oscillation of a wing and hovering rotating wings to a reasonable accuracy. Furthermore, results of this study indicate that most of the dominant aerodynamic effects of simple rotor in forward flight and rotor/body interaction phenomena can be estimated with this model.

Keywords : helicopter, rotor, aerodynamics, unsteady, panel method, numerical simulation.

1. INTRODUCTION

The first flying machine that was envisioned by the people of long ago was thought of as a vehicle that could fly just like a bird, that is, a machine with which they could take off, land and hover wherever they wished. Today, this type of aircraft configuration is a reality almost exclusively in the form of a helicopter.

The analytical study of helicopter rotary wing aerodynamics was limited until the maturity of the practical computer in the 1960s. The lifting line theory was used for blades and realistic representation of aerodynamic loadings was made possible [1]. By the end of the decade, Hess and Smith developed a technique to predict the flow velocity on non-lifting bodies [2]. This method was called the Panel Method and was derived from the classical potential flow theory. It utilized a distribution of singularities over an arbitrary body surface.

With more sophisticated computational facilities available today, aerodynamic force on very complex geometries and flight conditions can be computed.

One of the recent technological interest is unsteady aerodynamics. This area is especially significant in rotorcraft engineering because even in a steady translating flight, the helicopter creates an unsteady and complex make [3]. The rotating blades of a helicopter are exposed to a complex unsteady flow field due to the applied control inputs, motion of the blades, and the local changes in inflow velocity from the complex three-dimensional vortex wake shapes [4].

Related to this study is the interactional aero dynamics which is an attempt to understand the flow field around the complete helicopter. It is well known that mutual aerodynamic interference by components (main rotor, fuselage, tail rotor, etc.) of a helicopter has important effects on its flight performance.

In this project, an unsteady vortex wake model[5] was used along with a low order panel method code, PMARC (Panel Method Ames Research Center) [6]. This combination allows for the computation of aero dynamic forces during the low speed($M \ll 1$) unsteady motion of bodies without making assumptions about the wake shed from the trailing edges of wings.

The computational methed was validated and tested

*川田工業㈱ロサンゼルス事務所

for cases such as a sudden forward motion of a rectangular wing, pitch oscillations of an airfoil, and a hovering rotor. Furthermore, the applicability of the method to helicopter aerodynamics was demonstrated by testing the cases of a forward translating rotor and a rotor/body interaction.

This report is based on the author's master's thesis for San Diego State University, California, U.S.A. given in December, 1989.

2. THEORY

As shown in Fig-1, the origin of a body-fixed coordinate system (x,y,z) moves in the inertial coordinate system (X,Y,Z). The position and the momentary rotaion angles of the origin of the bodyfixed frame for $t>0$ relative to the inertial frame is given by $\vec{G}_1(t)$ and $\vec{G}_2(t)$ respectively.

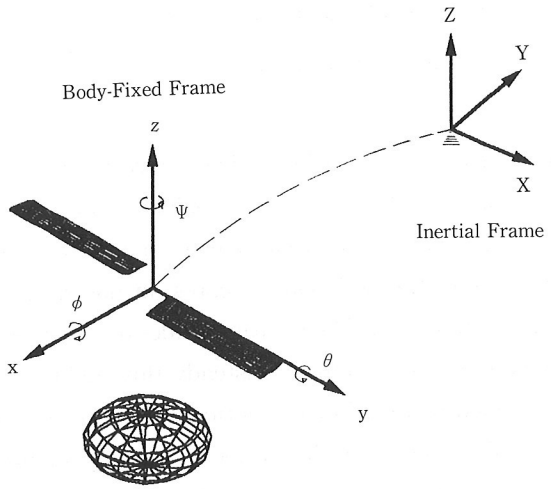

Fig-1. Coordinate Systems

$$\vec{G}_1(t)=(X_0, Y_0, Z_0) \quad \cdots\cdots(1)$$

$$\vec{G}_2(t)=(\phi,\theta,\psi) \quad \cdots\cdots(2)$$

It is assumed that the fluid (air) is inviscid, irrotational, and incompressible over the entire flow field except near the body's solid boundaries and its wakes. Based on these assumptions, a potential flow model can be used to calculate the pressure field due to this flow. In the inertial frame of reference, the continuity equation over the entire control volume is:

$$\nabla^2\Phi^*=0 \quad \cdots\cdots(3)$$

Superscript * indicates that this equation exists in the inertial frame. The flow is undisturbed at the far distance away from the body, thus:

$$\lim_{\vec{r}\to\infty}\nabla\Phi^*=0 \quad \cdots\cdots(4)$$

where $\vec{r}$ is the position vector (x, y, x). The air circulation $\vec{\Gamma}$ is conserved in the potential flow region, hence,

$$\frac{d\vec{\Gamma}}{dt}=0, \text{ for any } t \quad \cdots\cdots(5)$$

Since the viscosity terms are neglected, only one boundary condition, which is the zero normal velocity condition, is needed on the solid boundaries of the body. At any $t>0$,

$$(\nabla\Phi^*+\vec{v})\cdot\vec{n}=0 \quad \cdots\cdots(6)$$

where $\vec{v}$ is kinematic velocity of the body and $\vec{n}$ is the normal vector to the surface of the body. The solution is sought in the body-fixed coordinate system. The transformation of the position vector between the body-fixed and the inertial coordinate system is

$$\begin{Bmatrix} x \\ y \\ z \end{Bmatrix} = f(X_0, Y_0, Z_0, \phi, \theta, \Psi) \begin{Bmatrix} X \\ Y \\ Z \end{Bmatrix} \quad \cdots\cdots(7)$$

The transformation of the velocities between the two coorinate systems becomes

$$\vec{v}=\vec{V}_0+\vec{v}_{rel}+\vec{\Omega}\times\vec{r} \quad \cdots\cdots(8)$$

where $\vec{V}_0$ is the velocity of the origin of the body fixed coordinate system, $\vec{v}_{rel}$ is relative velocity measured by in the body-fixed frame, and $\vec{\Omega}$ is the rotation rate of the body-fixed coordinate. In this coordinate system, the continuity and far field equations remain unchanged, thus,

$$\nabla^2\Phi=0 \quad \cdots\cdots(9)$$

and

$$\lim_{\vec{r}\to\infty}\nabla\Phi=0 \quad \cdots\cdots(10)$$

The boundary condition becomes

$$(\nabla\Phi-\vec{V}_0-\vec{v}_{rel}-\vec{\Omega}\times\vec{r})\cdot\vec{n}=0 \quad \cdots\cdots(11)$$

The speed of sound is infinite in the potential flow, thus, the effect of the boundary condition at one moment is felt by the entire fluid region without any time delay. Therefore, for incompressible flow, the instantaneous solution is time independent. By substituting the boundary condition at each moment, a steady state solution technique can be used to solve the time dependent problem.

The flow must leave and airfoil's trailing edge smoothly in acoordance with the Kutta condition.

$$\nabla\Phi_{T.E.}<\infty \quad \cdots\cdots(12)$$

Unfortunately, the wake shape does depend on the history of the motion. Therefore, it is required to develop an adequate vortex wake model. Starting with the first time step, the wake panel elements are shed from the trailing edges of wings. In this case, it is assumed that the initial wakes from the trailing edges of wings are shed at a median angle $\delta_{T.E.}/2$ and are parallel to the free stream from then on. The vortex wake shape is obtained by adding wake panels at each time interval Δt. The vortex roll up is achieved by the wake corner points $(X,Y,Z)_i$ being transported by the local velocity $(U,V,W,)_i$ created by the body and its wake. The displacement of corner points between each time step is

$$\begin{pmatrix}\Delta x\\ \Delta y\\ \Delta z\end{pmatrix}_i=\begin{pmatrix}U\\ V\\ W\end{pmatrix}_i\cdot\Delta t \quad \cdots\cdots(13)$$

The wake strength is determined by applying the Kutta condition along the trailing edges of lifting wings. The Kelvin condition is used to calculate the change in the wake's streamwise circulation. Laplace's equation(9)can be solved by using Green's identity. The general solution is obtained by integrating the contributions of the source strength σ and doublet strength μ distributions over the body's surface and its wakes :

$$\Phi(x,y,z)=\frac{1}{4\pi}\int_{body+wake}\left[\mu\vec{n}\cdot\nabla\left(\frac{1}{r}\right)\right]dS-\frac{1}{4\pi}\int_{body}\sigma\left(\frac{1}{r}\right)dS \quad \cdots\cdots(14)$$

where S is the configuration surface element. The above equation is differentiated with respect to the body coordinates to fulfill the boundary condition. This operation results in the velocity induced by the doublet and source distributions :

$$\nabla\Phi=\frac{1}{4\pi}\int_{body+wake}\mu\nabla\left[\frac{\partial}{\partial n}\left(\frac{1}{r}\right)\right]dS-\frac{1}{4\pi}\int_{body}\sigma\nabla\left(\frac{1}{r}\right)dS \quad \cdots(15)$$

By substituting equation (15) into equation (11), the final equation is obtained.

$$\frac{1}{4\pi}\left\{\int_{body+wake}\mu\left[\frac{\partial}{\partial n}\left(\frac{1}{r}\right)\right]dS-\int_{body}\sigma\left(\frac{1}{r}\right)dS-\vec{V}_0-\vec{v}_{rel}-\vec{\Omega}\times\vec{r}\right\}\cdot\vec{n}=0 \quad \cdots\cdots(16)$$

The body surface separates the inner region of the body from the rest of the flow field external to the body. From the boundary conditions, this inner potential is set equal to the free stream value Φ_∞. Then equation (14) becomes

$$\frac{1}{4\pi}\int_{body+wake}\mu\left[\frac{\partial}{\partial n}\left(\frac{1}{r}\right)\right]dS-\frac{1}{4\pi}\int_{body}\sigma\left(\frac{1}{r}\right)dS=0 \quad \cdots(17)$$

It is assumed that the source strength at each panel is set equal to the normal component of local onset velocity. Then the value of the source distribution is

$$\sigma=\vec{n}\cdot(\vec{V}_0+\vec{\Omega}\times\vec{r}) \quad \cdots\cdots(18)$$

The surface of the body and its wake are broken up into discrete quadrilateral panels and it is assumed that the doublets and sources have constant strength on each panel. At each time step, the Kutta condition is applied and the wake is constructed progressively so the wake doublet strength μ_{wi} is known from the previous step. Now, the potential and induced velocity at a point is the summation of influences from all the panels. Substituting $\nabla\Phi$ from equation (15) into the boundary condition of equation (11) and evaluating the equation at the center point of each panel, the following simultaneous equations result.

$$[A_{i,j}]\begin{pmatrix}\mu_1\\ \mu_2\\ \cdot\\ \cdot\\ \cdot\\ \mu_k\end{pmatrix}=[B_{i,j}]\begin{pmatrix}\sigma_1\\ \sigma_2\\ \cdot\\ \cdot\\ \cdot\\ \sigma_k\end{pmatrix}+[C_{i,j}]\begin{pmatrix}\mu_{w1}\\ \mu_{w2}\\ \cdot\\ \cdot\\ \cdot\\ \mu_{w1}\end{pmatrix}+\begin{pmatrix}(v\cdot n)_1\\ (v\cdot n)_2\\ \cdot\\ \cdot\\ \cdot\\ (v\cdot n)_k\end{pmatrix} \quad \cdots\cdots(19)$$

where the subscripts k and l refer to the number of body panels and the number of wake elements, respectively. $[A_{i,j}]$, $[B_{i,j}]$, and $[C_{i.j}]$ are the influence coefficients corresponding to body doublet strentgth, body source strength, and wake doublet strength. The body matrices $[A_{i,j}]$ and $[B_{i,j}]$ are square matrices and have $k\times k$ elements. The number of elements in the wake matrix $[C_{i,j}]$ grows with each time step, therefore, the calculation becomes quite lengthy as more time steps are taken.

The pressure difference $p_\infty-p$ is calculated using Bernoulli's equation. In the inertial frame of reference,

$$\frac{p_\infty-p}{\rho}=-\frac{1}{2}\left[\left(\frac{\partial\Phi}{\partial x}\right)^2+\left(\frac{\partial\Phi}{\partial y}\right)^2+\left(\frac{\partial\Phi}{\partial z}\right)^2\right]+\frac{\partial\Phi}{\partial t} \quad \cdots(20)$$

In the body fixed frame the expression becomes :

$$\frac{p_\infty - p}{\rho} = -\frac{1}{2}\left[\left(\frac{\partial \Phi}{\partial x}\right)^2 + \left(\frac{\partial \Phi}{\partial y}\right)^2 + \left(\frac{\partial \Phi}{\partial z}\right)^2\right] + (\vec{V}_0 + \vec{\Omega} \times \vec{r}) \cdot \nabla \Phi + \frac{\partial \Phi}{\partial t} \quad \cdots\cdots(21)$$

Aerodynamic forces and moments can be obtained once the pressure field is known.

3. RESULTS AND DISCUSSION

As the first test case for the time dependent feature of the code, the sudden forward motion of a wing was investigated. The wing which is initially at rest is suddenly moved at a constant velocity V_∞ in the negative x-direction at $t > 0$. The motion of the body-fixed frame is given by

$$\vec{G}_1(t) = V_\infty \begin{pmatrix} 1 \\ 0 \\ 0 \end{pmatrix}, \text{ for } t > 0 \quad \cdots\cdots(22)$$

For this example, an NACA0012 airfoil shape at an angle of attack $\alpha = 5.0°$ is used. In the chordwise direction, 10 panels on each of the upper and lower surfaces describe the arifoil shape. A finite length rectangular wing of $AR = 6$ was given 10 panels across the half-span. The dimensionless velocity $V_\infty = 1.0$ was used. Wake shed by this movement is shown in Fig-2. In this figure, wing tip vortices are shown very well. The lift coefficient development history after a plunging motion is shown in Fig-3. Comparison with published results [7,8] shows that the values obtained by the current method agree well with the previous results.

To further check the validity of the method, the lift and pitching moment for an NACA0012 airfoil were tested for a pitch oscillation cycle. The oscillation of the airfoil about its quarter-chord is governed by the following equation.

$$\alpha = \alpha_0 + \alpha_1 \cdot \sin(\omega t) \quad \cdots\cdots(23)$$

For this part of the exercise, $\alpha_0 = 3.0°$, $\alpha_1 = 10.0°$, and $V_\infty \Delta t / c = 2.0$ are used. The lift histogram, Fig-4, shows that the computed values are in very good agreement with the previous results. The direction of the counterclockwise hysteresis is also correct. The pitching moment histogram shown in Fig-5 does not predict the correct slope of the cycle and the values are less damped than the experimental results. This

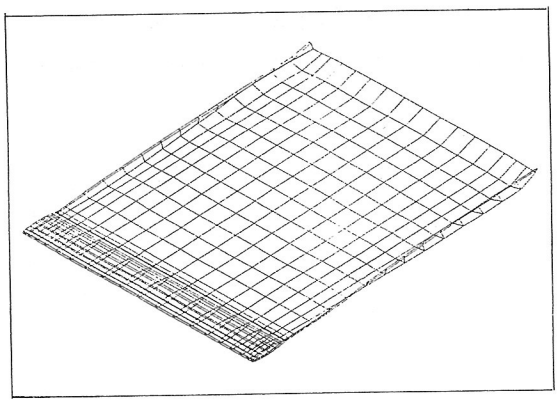

Fig-2. Wake Shed by a Sudden Forward Motion of a Rectangular Wing, $V_\infty \Delta t/c = 0.5$, 14th Time Stop

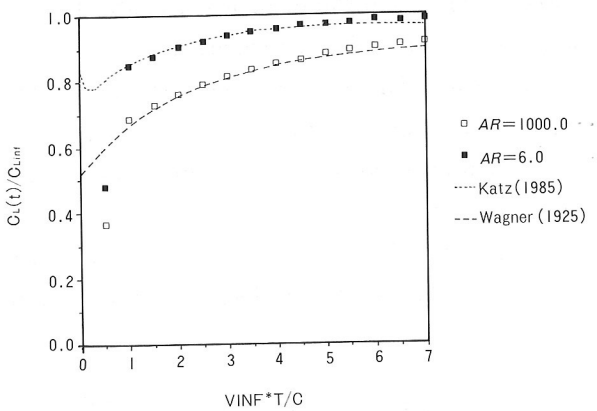

Fig-3. Life Coefficient Variation of a Sudden Forward motion of a Rectangular Wing

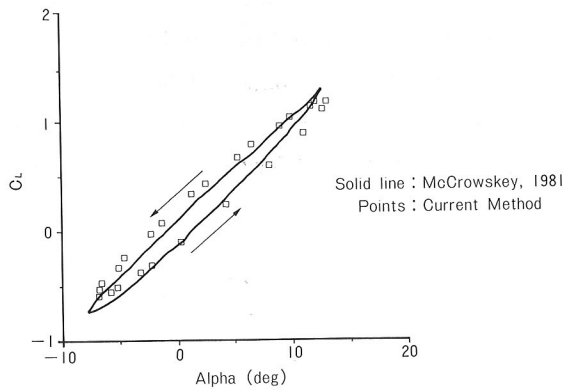

Fig-4. Lift Histogram for the Pitch Oscillations of an NACA0012 Airfoil

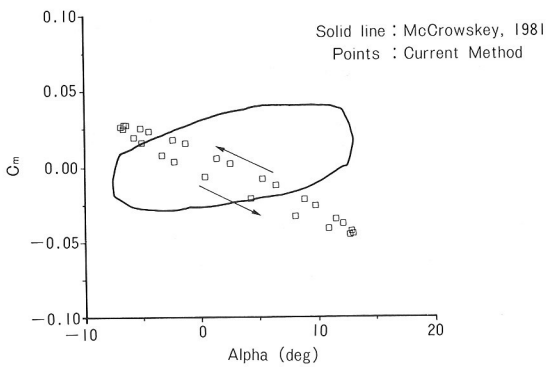

Fig-5. Pitch Moment Histogram for the Pitch Oscillations of a NACA0012 Airfoil

difference resulted from the center of pressure X_{cp} not being at the right position. However, the general shape and the direction of rotation of the pitching moment histogram are correct.

To simulate helicopter blade aerodynamics, the two rectangular wings were rotated around the z-axis. For the blades rotating at rate $\dot{\Psi}$, and encountering free stream velocity of V_∞ equations of motion are given by :

$$\vec{V}_0 = -\begin{pmatrix} V_\infty \\ 0 \\ 0 \end{pmatrix} \quad \cdots\cdots(24)$$

$$\vec{\Omega} = (0, 0, \dot{\Psi}) \quad \cdots\cdots(25)$$

An NACA0012 airfoil shape with $AR=5.0$ was used. For simplicity, the blades were taken to be rigid and untwisted. The wake shed by one blade was given an initial downward motion so it would not hit the other blade as it came around. In this case, the blades were given the collective pitch angle of $\alpha_R=8.0°$. The wake shed by a hovering rotor is shown in Fig-6. Since there was no translating motion, the wakes shown here are symmetric with respect to the z-axis for both blades. The calculated values used for the comparison with the experimental data of Caradonna and Tung[9] were taken from the 30th step for a time increment of $V_\infty \Delta t/c=2.0$.

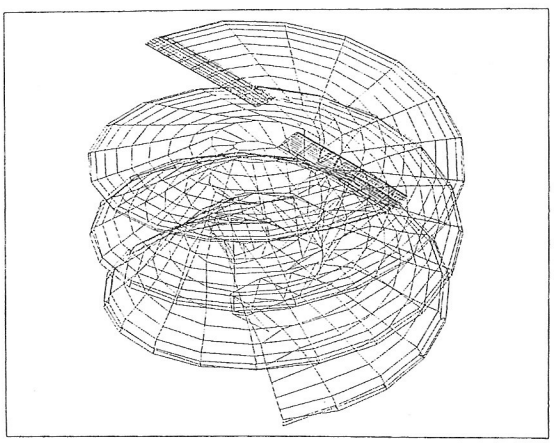

Fig-6. Wake Shed by a Hovering Rotor
$V_\infty \Delta t/c=2.0$, 30th Time Step

The chordwise loading at $r/R=0.5$ is shown in Fig-7. It can be seen that at the leading edge, the C_P compares fairly well to The experimental values but it deviates more and more as the station approaches the trailing edge. This disagreement arises from the initial downward motion of the wake and the wake not being fully developed at the time step the data were taken. It may also have been affected by the assumption that the wake is shed from the trailing edge with the initial angle of $\delta_{T.E.}/2.0$. This difference does not, however, seem to affect the code's ability to predict the spanwise lift distribution as much. The spanwise lift distribution after 30 time steps in Fig-8 shows that the calculated C_{lR} values follow the general shape of the experimental result. In this graph, the C_{lR} distribution line obtained by the code is above the experimental values. This difference also resulted from the underdeveloped wake.

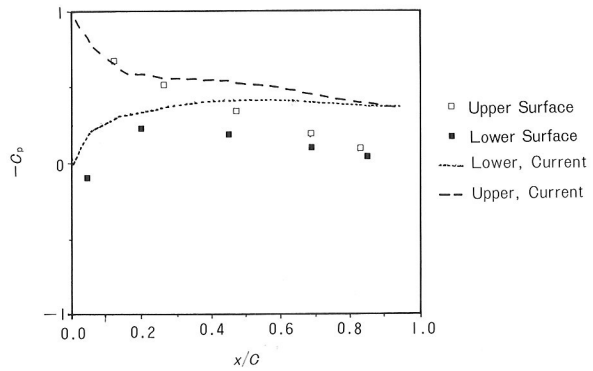

Fig-7. Chordwise C_P Distribution at $r/R=0.5$

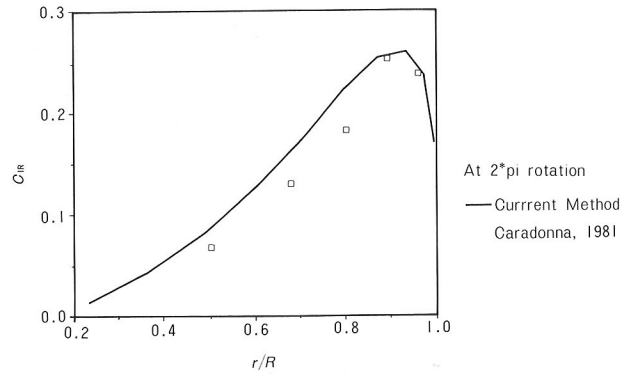

Fig-8. Spanwise Lift Distribution on a Helicopter Blade

As a more advanced appilcation of this code to helicopter aerodynamics, the low velocity forward flight situation (advance ratio $\mu_A=0.15$) was tested. The same two-bladed rotor configuration as the hovering rotor case was given the angle of attack of $\alpha=5.0°$. The lift history graph in Fig-9 shows, as expected, a sinusoidal type of a fluctuation with respect to the azimuth angle Ψ. Blade 1 correspond to the wing that is the original advancing blade and blade 2 is the original retreating blade. For this case, fluctu-

ation which is originally disturbed by the initial sudden movement becomes fairly smooth after $\Psi=225°$ (10 time steps). The coefficient of lift has the greatest value at the time the blade is forward sweeping and is at a right angle to the free-stream (i.e., $\Psi=0°$, 360°, 720°, etc. for Blade 1 and $\Psi=180°$, 540°, etc. for Blade 2) and decreases to the smallest value at the opposite side. The value becomes greater past this point and increases to the largest value at the original point. The spanwise loading distribution at various azimuth angles Ψ is shown in Fig-10. Here again, similar results were observed.

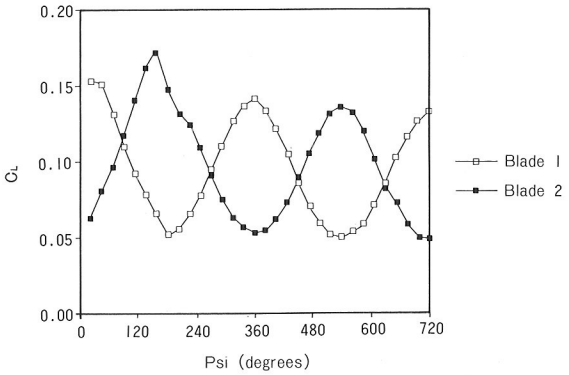

Fig-9. The Lift History of Two-Bladed Rotor in Forward Flight

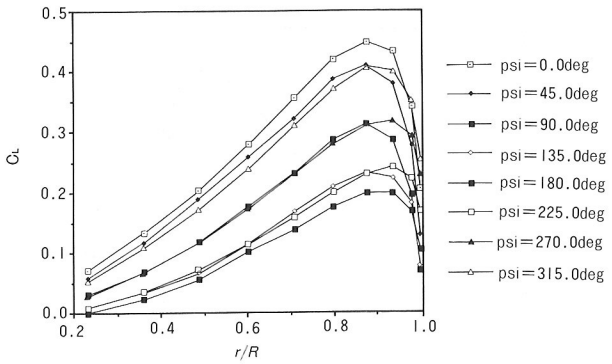

Fig-10. Spanwise Lift Distribution for Various Blade Azimuth Angle

Analytical studies of helicopter interactional aerodynamics has been mainly limited to that of the main rotor and the body. The applicability of this code to the interaction phenomena between the rotor and an ellipsoid was investigated. An ellipsoid which is symmetric with respect to the z-axis was placed below the blades (refer to Fig-11. For this case, the whole system, including the body was rotated around the z-axis. Although the angle of attack of 5.0° was given to the system, the coefficient of lift for the isolated body was practically zero for this advance ratio ($\mu_A=0.15$). Rotor/body separations of $h/R=10.0$, 5.0, 1.0 and 0.5 were tested. It is assumed that no wake is shed by the body. Wake shed by blades for $h/R=0.5$ case is shown in Fig-12. The blade C_L history of different rotor/body vertical separations superimposed on that of the blades alone is shown in Fig-13. From this graph, it is clear that the case for $h/R=0.5$ shows more disturbance in the fluctuating blade C_L history than for the $h/R=1.0$ case. Although there are no previous results that can be directly compared to this exercise, similar results were obtained by experiments [10,11,12]and by an analytical method[1].

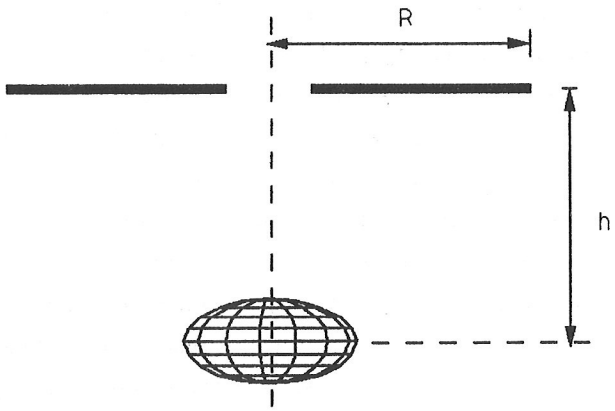

Fig-11. Rotor/Body Configuration

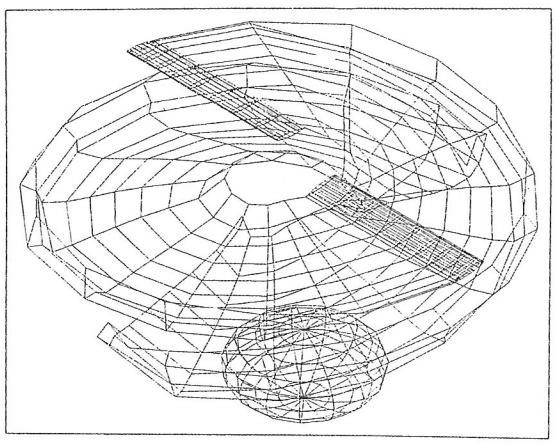

Fig-12. Wake Shed by Rotor Blades of Rotor/Body Configumation $h/R=1.0\Psi=270°$

4. CONCLUSIONS

In this study, an unsteady panel method code was verified and its applicability to helicopter aerodynamics was studied. The code uses a vortex wake method[6]along with a low order panel method, PMARC[7]. It was found that even when a large time increment was used, the code could predict the

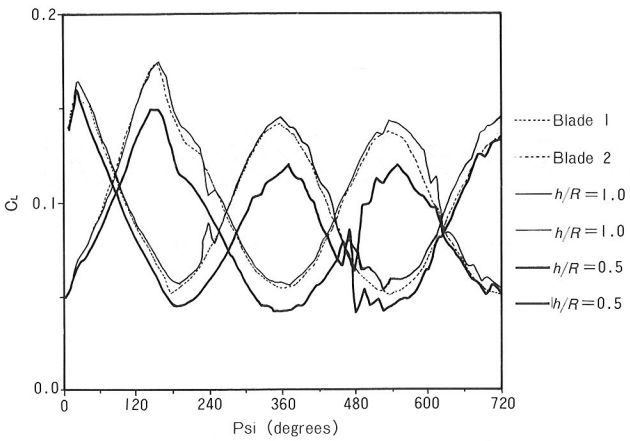

Fig-13. Blade Lift Histories of Rotor/Body Configuration Superimposed

unsteady aerodynamic forces for a sudden forward motion and a pitching oscillation of a wing and hovering rotating wings to a reasonable accuracy. Also, the results of this study indicate that most of the dominant aerodynamic effects of simple rotors in forward flight and rotor/body interaction phenomena can be estimated with this model. The code has a major advantage in that complex wake shapes are automatically developed so that the prescription of wake shapes as required by other methods is not necessary. It was shown that for low speed ($M \ll 1$) the values obtained by the current method compare well with experimental results with reasonable computational efficiency. A Micro VAX computer was sufficient for the analysis of the models studied in this paper and a supercomputer such as the Cray XMP was not needed.

REFERENCES

1) Clark, David R., Maskew, Brian : Calculation of Unsteady Rotor Blade Loads and Blade/Fuselage Interference, presented at the Second International Conference on Rotorcraft Basic Research, February, 1988.

2) Hess, J.L., and Smith, A.M.O. : Calculation of Potential Flow about Arbitrary Bodies, *Prog, Aeronaut, Sci.,* Vol. 8 , 1966, pp.1～138.

3) Johnson, Wayne : Recent Developments in Rotary-Wing Aerodynamic Theory, *AIAA Journal,* Vol.24, No.8, August, 1986, pp.1219～1244.

4) Leishman, J.G. and Beddoes, T.S. : A Semi-Empirical Model for Dynamic Stall, *Journal of American Helicopter Society,* Vol.34, No. 3, July, 1989, pp. 3～17.

5) Katz, J. and Maskew, B : Unsteady Low-Speed Aerodynamics Model for Complete Aircraft Configurations, AIAA-86-2180-CP, August, 1986.

6) Ashby, Dale L., Iguchi, Steven K., and Dudley, Michael : Development and Validation of an Advanced Low-Order Panel Method, NASA TM-101024, October, 1988.

7) Wagner, H . : Über die Entstehung des Dynamischen Auftriebes von Tragflügeln, *Z.F.A.M.M.,* Vol. 5, No. 1, February, 1925, pp.17～35.

8) Katz, J. : Calculation of the Aerodynamic Forces on Automotive Lifting Surfaces, *ASME Journal of Fluids Engineering, Vol.* 107, 1985, pp.438～443.

9) Caradonna, F.X. , and Tung, C. : Experimental and Analytical Studies of a Model Helicopter Rotor in Hover, NASA TM-81232, September, 1981.

10) Wilson John C. and Mineck, Raymond E. : Wind-Tunnel Investigation of Helicopter-Rotor Wake Effects on Three Helicopter Fuselage Models, NASA TM X-3185, March, 1975.

11) Smith, Charles A. and Betzina, Mark D. : Aerodynamic Loads Induced by a Rotor on a Body of Revolution, *Journal of American Helicopter Society,* January, 1986, pp.29～36

12) Leishman. J. G. : Studies in Rotor/Airframe Interactional Aerodynamics at the University of Maryland, presented at ARO Interactional Aerodynamic Workshop, U.S. Army Research Office, July, 1988.